Targeting the Lysosome: Fluorescent Iron(III) Chelators To Selectively Monitor Endosomal/Lysosomal Labile Iron Pools

Sarah Fakih,*[,†] Maria Podinovskaia,[§] Xiaole Kong,[‡] Helen L. Collins,[#] Ulrich E. Schaible,[§] and Robert C. Hider[‡]

Division of Pharmaceutical Sciences, King's College London, Franklin-Wilkins-Building, Stamford Street, London SE1 9NH, U.K., Department of Inorganic Chemistry, Georg-August University of Göttingen, Tammannstrasse 4, 37077 Göttingen, Germany, Department of Infectious and Tropical Diseases, London School of Hygiene and Tropical Medicine, Keppel Street, London WC1E 7HT, U.K., and Department of Infectious Diseases, King's College London, Hodgkin-Building, Guy's Campus, London SE1 1UL, U.K.

Received February 6, 2008

Iron-sensitive fluorescent chemosensors in combination with digital fluorescence spectroscopy have led to the identification of a distinct subcellular compartmentation of intracellular redox-active "labile" iron. To investigate the distribution of labile iron, our research has been focused on the development of fluorescent iron sensors targeting the endosomal/lysosomal system. Following the recent introduction of a series of 3-hydroxypyridin-4-one (HPO) based fluorescent probes we present here two novel HPO sensors capable of accumulating and monitoring iron exclusively in endosomal/lysosomal compartments. Flow cytometric and confocal microscopy studies in murine macrophages revealed endosomal/lysosomal sequestration of the probes and high responsiveness toward alterations of vesicular labile iron concentrations. This allowed assessment of cellular iron status with high sensitivity in response to the clinically applied medications desferrioxamine, deferiprone, and deferasirox. The probes represent a powerful class of sensors for quantitative iron detection and clinical real-time monitoring of subcellular labile iron levels in health and disease.

Introduction

Iron is the most abundant transition metal in cellular systems holding an outstanding biological importance because of its presence in the structures of numerous enzymes and proteins.[1,2] By virtue of its facile redox chemistry and its high affinity for oxygen, iron is critically involved in electron transfer reactions as well as oxygen transport. In contrast to iron bound to proteins, the intracellular labile iron pool has a considerable toxic potential. In the presence of reactive oxygen species (ROS) loosely bound iron is able to redox cycle between its most stable oxidation states Fe(II)/Fe(III), catalyzing the formation of oxygen-derived free radicals such as the hydroxyl radical via the Fenton reaction.[3,4] These highly reactive radical species are capable of interacting with most types of biological material including sugars, lipids, proteins, and nucleic acids. The resulting injurious processes covering lipid peroxidation, protein oxidation, DNA/RNA oxidation, and DNA lesions take a critical lead in the development of pathology in diseases such as hepatitis, hemochromatosis, liver cirrhosis, cancer, and neurodegeneration.[3,5–12]

Labile iron is generally considered to be cytosolic, its uptake being driven by receptor-mediated endocytosis of transferrin-bound iron. However, increasing experimental evidence assigns only a minor fraction of the total cellular redox-active iron to the cytosol. Rapid transit of the metal to dominant sites of iron sequestration and incorporation into proteins can relocate cytosolic iron to distinct subcellular compartments.[13]

Considerable accumulation of redox-active iron in the lysosomal system provided by high turnover degradation of endocytosed as well as autophagocytosed iron-containing macromolecules creates a highly potent source of intracellular oxidative potential.[14] Consequently, exposure to intracellular ROS renders these organelles particularly susceptible to oxidative damage. Organelle rupture resulting from intralysosomal Fenton reactions during oxidative stress situations has been associated with enhanced DNA damage due to the sudden release of lysosomal labile iron into the cytoplasm.[15,16] Permeabilization of mitochondrial membranes by released lysosomal enzymes most likely induces a loss of mitochondrial membrane potential, irreversibly leading to cell death.[14,17–19] Administration of the lipophilic chelator salicylaldehyde isonicotinoyl hydrazone (SIH[a]) has been shown to provide protection against oxidative stress-induced cell death by virtue of its strong iron chelating properties.[20,21] Correspondingly, the predominantly lysosomal high-affinity iron chelator desferrioxamine (DFO) sustains lysosomal stability during oxidative stress, preventing organelle rupture, DNA damage, loss of mitochondrial membrane potential, and cell death.[16,18,19]

Most methods to characterize intracellular labile iron distribution seriously perturb the extent and nature of the labile iron pool, rendering them inapplicable to living cells. In combination with noninvasive and high resolution confocal imaging, fluorescent chemosensors have proven to be highly sensitive tools to investigate the metabolism of labile metal pools in individual cells with subcellular resolution.[13,22–27] To the best of our knowledge, a fluorescent probe selectively accumulating inside the endosomes/lysosomes to allow monitoring of labile iron has not been available to date. To investigate the chemical nature of intracellular labile iron pools, we recently introduced a series of coumarin labeled fluorescent 3-hydroxypyridin-4-one (HPO) based probes for imaging and quantification of cytosolic labile iron.[28–30] Here, we report the synthesis and functional characterization of two novel fluorescein labeled 3-hydroxypyridin-4-one based fluorescent probes to monitor endosomal/lysosomal

* To whom correspondence should be addressed. Phone: +49 (0)551 39 3006. Fax: +49 (0)551 39 3363. E-mail: sarah.fakih@chemie.uni-goettingen.de.

† Georg-August University of Göttingen.

§ London School of Hygiene and Tropical Medicine.

‡ Division of Pharmaceutical Sciences, King's College London.

Department of Infectious Diseases, King's College London.

[a] Abbreviations: HPO, 3-hydroxypyridin-4-one; SIH, salicylaldehyde isonicotinoyl hydrazone; DFO, desferrioxamine; BMM, bone marrow macrophages; DFR, deferasirox; DFP, deferiprone; DexTR, dextran Texas Red; FeDex, iron(III) dextran.

10.1021/jm8001247 CCC: $40.75
Published on Web 07/15/2008

Scheme 1. Synthesis of the Fluorescent Probe **9**

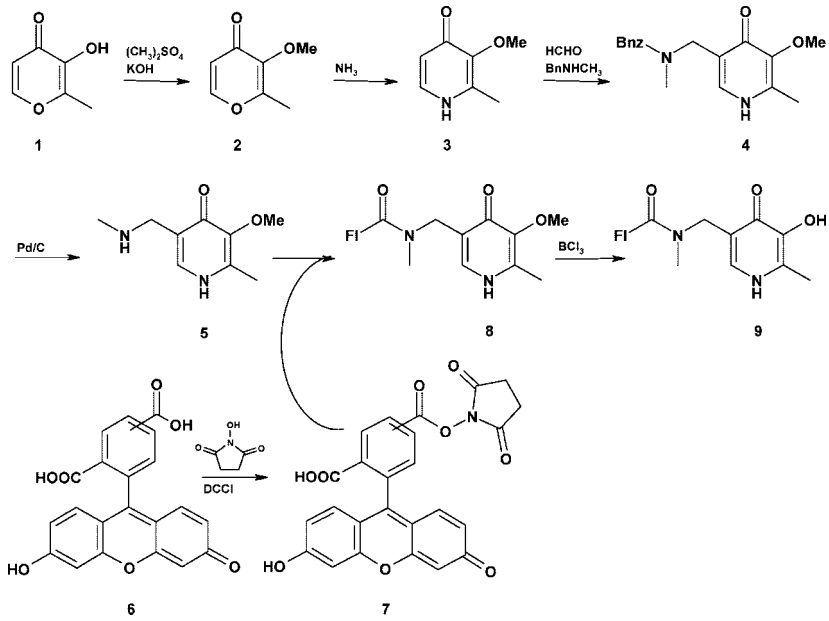

Scheme 2. Synthesis of the Fluorescent Probe **20**

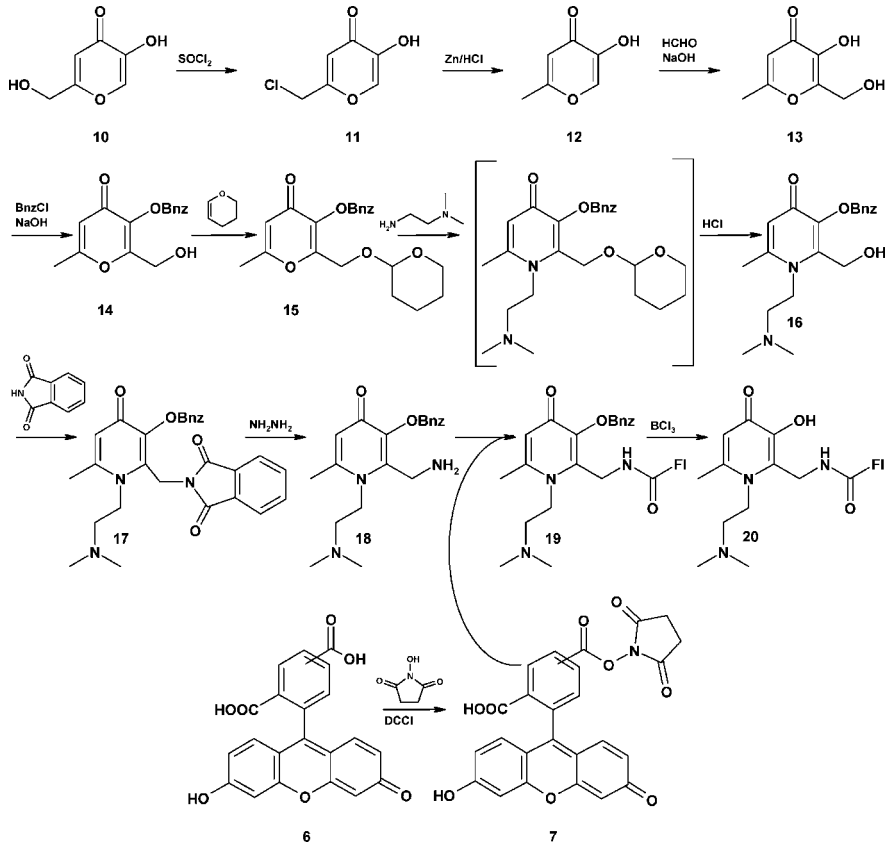

iron. We analyzed the physicochemical properties of these probes regarding their sensitivity toward ferric iron. Intracellular distribution and responsiveness to drug mediated modifications of iron concentrations have been investigated in murine bone marrow derived macrophages using flow cytometry and confocal microscopy.

Results and Discussion

Chemistry. The structures of the HPO-based fluorescent iron chemosensors **9** and **20** are illustrated in Schemes 1 and 2. Intracellular distribution properties of HPO-based compounds have been found to be regulated mainly by the chemical nature of the substituent at the nitrogen atom in the 1-position. Probe **9** featuring an unsubstituted nitrogen atom in the 1-position was designed to function as a nonspecific sensor with no selective intracellular distribution pattern. Probe **20** on the other hand was designed as a lysosomotrophic sensor based on the structural incorporation of a basic 1-dimethylethylamine substituent. Because of the acidic nature of endosomal/lysosomal compartments, probes featuring basic moieties undergo rapid protonation

following their uptake into the vesicles. The resulting charged molecule species are trapped inside the vesicles because of their relative membrane impermeability, providing for an efficient intraorganelle enrichment with the compound.[31]

Syntheses of compounds **2**−**5** and **11**−**14** were based on procedure described previously.[28] Scheme 1 illustrates the synthetic route employed for the preparation of the 5-fluorescein labeled probe **9** starting from commercially available 3-hydroxy-2-methyl-4*H*-pyran-4-one (maltol, **1**). Protection of the 3-hydroxyl group was achieved by methylation using dimethyl sulfate under basic conditions and was followed by exchange of the ring oxygen with nitrogen via reaction with aqueous ammonia solution to obtain 3-methoxy-2-methylpyridin-4(1*H*)-one **3**. Aminomethylation of the activated 5-position was then accomplished by Mannich reaction conditions using formaldehyde and *N*-benzylmethylamine. Subsequent removal of the benzyl protection group via hydrogenation yielded the functionalized 3-methoxy-2-methyl-5-[(methylamino)methyl]pyridin-4(1*H*)-one **5** furnished with a secondary amine in the 5-position, which is suitable for fluorophor coupling. The coupling of fluorescein to the protected pyridinone **5** proceeded via preceding activation of commercially available 5(6)-carboxyfluorescein **6** to yield **7** using *N*-hydroxysuccinimde and the peptide coupling reagent dicyclohexylcarbodiimide (DCCI). Following fluorophor coupling, deprotection of the methyl protected 3-hydroxyl group of **8** was achieved by reaction with BCl_3, furnishing the fully functional iron(III) sensitive fluorescence chemosenor **9**.

The fluorescein labeled probe **20** was prepared following a multistep synthesis strategy summarized in Scheme 2. Starting from 5-hydroxy-2-(hydroxymethyl)-4*H*-pyran-4-one (kojic acid, **10**), the 2-hydroxymethyl residue was converted into a methyl group via preceding chlorination using thionyl chloride (**11**) followed by reduction using zinc powder and concentrated hydrochloric acid to yield 5-hydroxy-2-methyl-4(1*H*)-pyran-4-one **12**. Reaction with formaldehyde under basic conditions resulted in a hydroxymethyl substituent in the 6-position (**13**). After benzylation of the 3-hydroxyl group (**14**), the ring oxygen was exchanged with dimethylethylenediamine to yield **16** following intermediate formation of the 2-tetrahydropyrane protected 3-(benzyloxy)-6-methyl-2-[(tetrahydro-2*H*-pyran-2-yloxy)methyl]-4*H*-pyran-4-one **15**. Conversion of **16** to the corresponding phthalimido derivative proceeded via the Mitsunobu reaction using phthalimide, triphenylphosphine, and diisopropyl azodicarboxylate. The quaternary phosphonium salt forming upon reaction of triphenylphosphine with diisopropyl azodicarboxylate is protonated by the nucleophilic phthalimide and activates the 2-hydroxyl substituent through formation of an alkoxyphosphonium salt. Nucleophilic substitution of the phosphonium moiety by the deprotonated phthalimide furnishes the desired phthalimide derivative **17**.[32] Subsequent hydrazinolysis of **17** yielded 2-(aminomethyl)-3-(benzyloxy)-1-[2-(dimethylamino)ethyl]-6-methylpyridin-4(1*H*)-one **18** functionalized in the 2-position with a primary amine for fluorophor coupling. Coupling of the activated 5(6)-carboxyfluorescein *N*-hydroxysuccinimide ester **7** with **18** furnished the protected probe precursor **19**, which was converted to the functional iron(III) chemosensor **20** by debenzylation of the 3-hydroxyl group via hydrogenolysis.

Optical Characterization. The applicability of a fluorescent chemosensor to monitor the metabolism and translocation dynamics of intracellular labile cations is essentially based on the responsiveness of its fluorophor unit toward the presence of the targeted ion. Binding of iron to the HPO chelation moiety of the fluorescent probes **9** and **20** induces quenching of the fluorescein fluorophor unit depending on the available Fe(III) concentration. By virtue of the excellent iron selectivity of the HPO binding moiety, interfering signaling by other biologically active metals can be mostly precluded. The HPO based fluorescent sensors specifically do not suffer from interference from zinc, calcium, and magnesium.[29,33] Appreciable interference has been observed in the presence of Cu(II). Yet copper is known to be chaperoned very tightly in mammalian cells by copper-binding proteins and other ligands. Consequently, the intracellular labile copper pool is vanishingly small (less than a single solvated copper ion per cell) and can in practice be neglected.[34] To confirm HPO characteristic Fe(III) selectivity for the presented fluorescein coupled sensors, representative interaction of **9** with Ca(II), Mg(II), Cu(II), Ni(II), Zn(II), Mn(II), and Co(II) was recorded and confirmed fluorescence insensibility toward the tested metals except for the expected quenching effect (32.3%) in the case of Cu(II) (data see Supporting Information).

Illustrated in Figure 1 is a representative fluorescence emission profile of probe **20** titrated with increasing Fe(III) concentrations as well as a comparative plot of the averaged quenching capacities of both probes. Owing to the fluorescein moiety, characteristic excitation maxima for **9** and **20** are at 494 and 491 nm while emission maxima are at 512 and 514 nm. All measurements were carried out at pH 7.4 in Chelex-treated MOPS buffer to avoid interfering quenching signals by iron contamination. Titration of the iron-free buffered probe solutions with increasing Fe(III) concentrations showed an overall quenching capacity of 77% for **9** and a notably higher quenching capacity of 96% for **20**. Both quenching profiles stabilize at an iron concentration of ∼1 μM, indicating completed iron complex formation. In view of the applied 3 μM sensor concentration, the resulting 3:1 probe/metal molar ratio at fluorescence stabilization suggests binding of three bidentate HPO chelators, required to form the anticipated fully coordinated octahedral iron(III) complex.

Dequenching kinetics of Fe(III) complex solutions of **9** and **20** were investigated using the HPO-based nonfluorescent chelator 1,2-diethyl-3-hydroxypyridin-4(1*H*)-one (CP94) and the high-affinity iron chelator SIH, exhibiting pFe^{3+} values of 19.7 (CP94)[35] and 50 (SIH),[36] respectively. Illustrated in Figure 2 is the representative time-dependent dequenching profile of the Fe(**20**)$_3$ complex employing each dequencher, expressed as a percentage of the initial sensor fluorescence in the absence of iron (set at 100%). By virtue of its higher Fe(III) binding constant, SIH rapidly restores 95% of the initial fluorescence of **20** (**9**, 92%, data not shown) while 87% recovery can be achieved applying CP94 (**9**, 87%, data not shown). Optical properties of both sensors are summarized in Table 1.

pH Sensitivity. For biological application of the sensors and data analysis on the basis of specific fluorescence emission intensities, it is necessary to consider the intrinsic pH sensitivity of fluorescein. In solution fluorescein can in principle exist in four different prototropic forms, covering the cation, the neutral molecule, the monoanion, and the dianion.[37] Because of complex prototropic equilibria, spectral properties of fluorescein are particularly sensitive to pH. In the pH range 6−10, species distribution is dominated by the monoanion−dianion equilibrium; the cation and neutral species virtually do not exist.[38,39] As primarily the dianion accounts for the observed fluorescence intensity at pH 7.4,[38,40] the fluorescence emission spectrum shows a significant decrease of emission intensity at low pH. A representative pH titration of **20** in Chelex-treated buffer

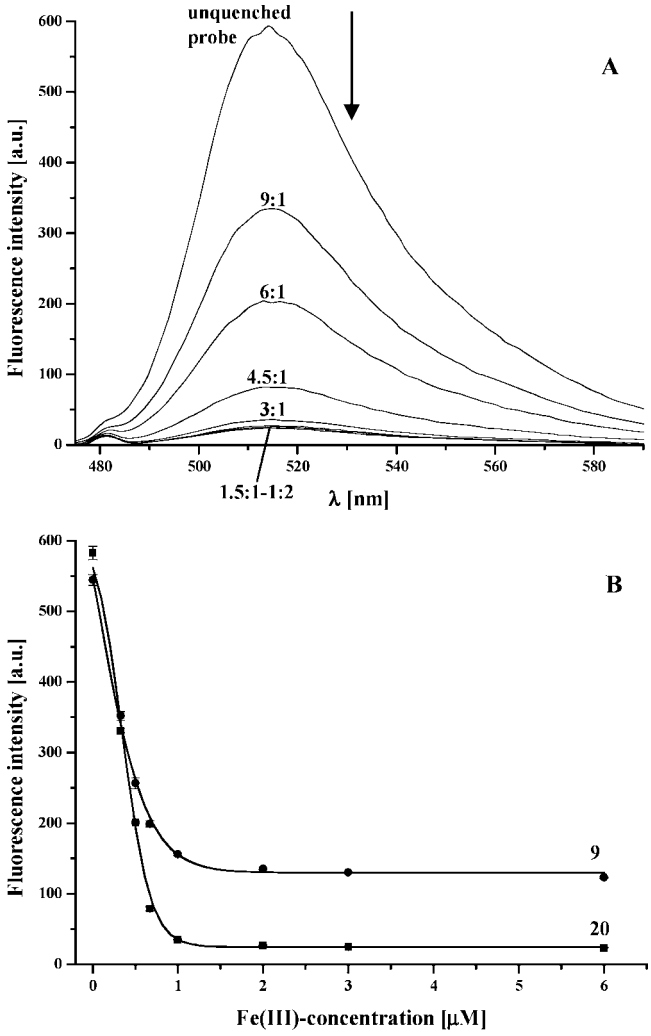

Figure 1. (A) Representative fluorescence emission profile of **20** in the presence of increasing Fe(III) concentrations (arrow). Fe(III) atomic absorption spectroscopy standard solution was mixed with NTA in a 1:5 molar ratio prior to the measurements. Quenching was carried out by titration of a probe solution (3 μM) in Chelex-treated MOPS buffer (50 mM) at pH 7.4 with a series of Fe(III)/NTA concentrations resulting in probe/metal ratios of 9:1, 6:1, 4.5:1, 3:1, 1.5:1, 1:1, and 1:2. Fluorescence was excited at 491 nm. (B) Fluorescence intensity maxima (514 nm) of the quenching spectra plotted against corresponding Fe(III) concentrations. Measurements were carried out in triplicate. Data shown represent mean values ± SEM.

(Figure 3) illustrates the decrease of sensor fluorescence upon acidification in relation to the highest observed fluorescence at pH 7.4 set at 100%. The pH profile of **20** revealed a 15−67% decrease in fluorescence intensity between pH 7.4−6 and pH 6−4.5, respectively, corresponding to the region of pH changes that can be anticipated during transitions of early endosomes to late endosomes/lysosomes.

Physicochemical Characterization. The specific solution properties of the fluorescent sensors **9** and **20** were investigated using an automated spectrophotometric titration system. The UV/vis profile of the iron free sensor **20** measured over the pH range 1.65−11.16 is illustrated in Figure 4 together with the speciation plot derived from the detected spectral changes. As shown for **20**, both probes exist predominantly as the 3-protonated LH species at pH 7.4 (**9**, 93.0%; **20**, 88.9%), thus forming neutral tris-Fe(III) complexes with intracellular labile iron under physiological conditions. The affinity of both compounds for Fe(III) reflects the combined pK_a values of the chelating oxygen

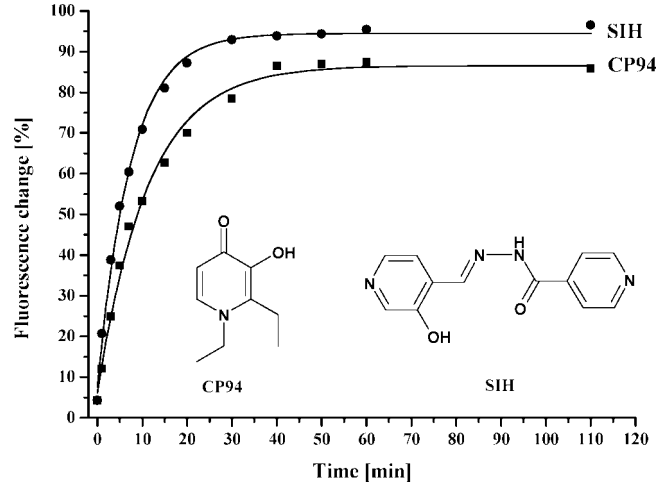

Figure 2. Comparative plot of the dequenching kinetics of the fully quenched Fe(**20**)$_3$ complex in Chelex-treated MOPS buffer (50 mM) at pH 7.4. The iron complex was prepared from a 3 μM sensor solution and a 3 μM NTA-buffered iron(III) solution (iron/NTA, 1:5 molar ratio). Application of the nonfluorescent iron(III) chelators CP94 (1 mM) and SIH (100 μM) showed maximal dequenching capacities of 87% and 95%, respectively, indicated by stable plateau formation after approximately 40 min.

donors: 3-hydroxyl (p$K_a \approx 9.8$) and 4-carbonyl functions (p$K_a \approx 3.7$, pK_a values relating to 1,2-dimethyl-3-hydroxypyridine-4-one). The pK_a value of the carbonyl function results from extensive delocalization of the lone pair associated with the ring nitrogen. pK_a values of both sensor molecules as derived from the spectrophotometric titration are listed in Table 1. For **9** and **20** the oxygen atom of the 3-hydroxyl function shows values of 9.91 and 9.29, respectively, and the corresponding values for the oxygen atom of the 4-carbonyl function are 3.85 and 3.81.

Considering the representative speciation plot of **20**, both fluorescent sensors exist as dianions at physiological pH because of the deprotonated phenol and carboxyl functions of the fluorescein moieties, showing pK_a values of 6.26/1.91 for **9** and 6.44/2.01 for **20**. To assess membrane permeation qualities of the probes, the logarithm of the partition coefficient, log P, and the distribution coefficient, log $D_{7.4}$, were determined for both sensors (Table 1). The partition coefficient, representing the standard measure of lipophilicity, is determined by distribution of a compound between two phases (*n*-octanol/water) applying pH conditions providing for a neutral molecule. At pH 7.4 the neutral LH_3 sensor species of **9** and **20** represent only 0.0019% and 7.9% of the overall species composition but exist as the dominant species within the pH ranges of 2−4 (**9**) and 3.5−5.5 (**20**). While **20** exhibits a log P value of −0.35, **9** shows a surprisingly high log P value of 2.12, suggesting high membrane permeation qualities of its neutral molecule species. The striking difference between the log P values of **9** and **20** can be attributed to the additional functionalization of the HPO chelation unit of **20** in the 1-position. Introduction of the ethyl-bridged secondary amine strongly influences the overall polarity of the molecule and renders the probe significantly more hydrophilic than its unsubstituted analogue. On the basis of the log P measurements, the corresponding log $D_{7.4}$ values were calculated, quantifying the potential membrane permeation qualities of both probes under physiological conditions. Comparison of the log $D_{7.4}$ values of **9** (−2.61) and **20** (−3.03) with the clinically applied 3-hydroxypyridin-4-one analogue deferiprone (1,2-dimethyl-3-hydroxypyridine-4-one, log $D_{7.4} = -0.77$)[41] clearly reflects the magnitude of change in molecular polarity, primarily resulting

Table 1. Physicochemical Properties of the Fluorescent Probes **9** and **20**

	excitation λ (nm)	emission λ (nm)	ε [a] $\times 10^3$ m^{-1} cm^{-1}	quenching [Fe(III)] (%)	dequenching (SIH/CP94) (%)	pK_a	log P [b]	log $D_{7.4}$
9	494	512	49.6	77	92/87	9.91, 6.26, 3.85, 1.91	2.12	−2.61
20	491	514	60.1	96	95/87	9.29, 6.44 5.74, 3.81, 2.12	−0.35	−3.03

[a] Molar extinction coefficient; [b] Partition coefficient (citric acid buffer/*n*-octanol), measured at pH 3 (**9**) and pH 4.5 (**20**).

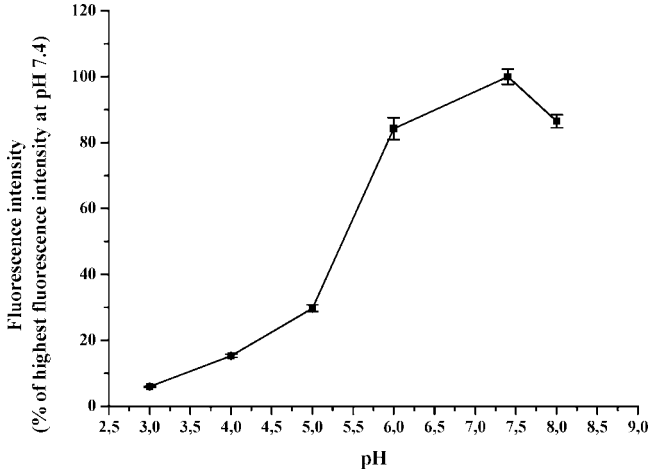

Figure 3. pH dependent fluorescence profile of **20**. The probe was measured at pH 3, 4, 5, 6, 7.4, and 8 in Chelex-treated buffer solutions (pH 3−6, citrate buffer 10 mM; pH 7.4, 8, MOPS buffer 50 mM). Shown are mean values ± SEM of triple measurements.

from coupling of the fluorescein fluorophor moiety. Thus, the low distribution coefficient further confirms the results obtained from spectrophotometric titrations characterizing both probes as highly hydrophilic and virtually membrane impermeable under physiological conditions.

Live Cell Measurements. The in vitro sensitivity of the fluorescein labeled probes was investigated by flow cytometry (FACS) analysis using bone marrow derived macrophages (BMMØ) from C57BL/6 mice. All FACS analyses were carried out in Chelex-treated PBS to avoid external iron contamination resulting in artificial quenching signals.

Representative for both probes, the intracellular responsiveness of **20** to changes of lysosomal iron concentrations was measured after cellular iron supplementation or deprivation. Endosomal/lysosomal iron concentrations were specifically altered using high molecular weight iron dextran and the membrane impermeable high affinity chelator desferrioxamine (DFO), both selectively accumulating in the endosomal/lysosomal compartments because of their cellular uptake route via endocytosis. Studies on cellular uptake kinetics of **9** and **20** showed optimal intracellular probe loading for FACS analysis after pulsing BMMØ with 5 μM probe in iron-free PBS for 20 min followed by a 1 or 2 h chase.[42]

The sensitivity of **20** to changes of intralysosomal iron concentrations was measured in comparison to its protected and therefore iron-insensitive fluorescent precursor **19** after 1 and 2 h. Flow cytometric histograms are presented in Figure 5. The fluorescent probe **19**, which is incapable of chelating iron, shows no response to manipulations of the endosomal/lysosomal iron content and exhibits constant fluorescence emission intensities under all conditions. The iron-sensitive probe **20**, however, shows increased fluorescence intensity in cells treated with the high-affinity iron chelator DFO in comparison to untreated cells. Correspondingly, decreased fluorescence intensity can be observed following subsequent addition of exogenous iron via iron dextran.

Fluorescence data acquired for the iron-sensitive probe **20** over the entire time-course of the experiments is shown in Figure 6. Curve progression indicates that dequenching/quenching processes passed through a maximum at 1 h. Converted to percentage changes of fluorescence emission intensities in relation to untreated **20**-stained cells (set at 0%), a 187.78 ± 52.78% fluorescence increase and a 67.33 ± 4.33% decrease after a 1 h treatment with DFO or iron dextran were recorded. Comparison of in vitro data for **20** with results for **9** (data not shown) showed a higher degree of in vitro responsiveness of **20**. Applying DFO or iron dextran for 1 h to **9**-stained BMMØ resulted in significantly lower dequenching (43.65 ± 7.83%) and quenching processes (41.58 ± 1.82%). This is in agreement with the superior optical properties of **20** (Figure 1B).

At 2 h after loading, the fluorescent signals of both sensors were reproducibly reduced when compared to the 1 h time point values. While **20** shows a considerable difference of 83.35% for dequenching and 11.75% for quenching signals, **9** exhibits less pronounced changes of 11.20% and 7.87%, respectively (data not shown). To evaluate possible changes in dequenching and quenching capacities with regard to intracellular fluorescence signals independent of DFO or iron dextran, fluorescence intensities of untreated cells stained with the fluorescent probes or their protected precursors **8** and **19** were compared over the entire 2 h incubation period as illustrated in Figure 7. Labeling with iron-sensitive or -insensitive probes lead to a constant intracellular fluorescence of labeled cells after reaching a steady quenching equilibrium. The data suggest that **20** has already reached a quenching equilibrium 20 min after loading (t = 0 min) while **9** has reached an equilibrium 1 h after loading. Thus, alterations of fluorescence intensities are independent of basal cellular fluorescence levels and can most likely be accredited to intracellular iron homeostasis kinetics. The differences between the fluorescence signals of the iron insensitive precursors compared to the iron sensors as illustrated in Figure 7 indicate quenching processes predominantly associated with iron chelation.

Constant fluorescence of the iron insensitive precursors **8** and **19** over the 2 h incubation period suggests that changes in fluorescence intensities due to a shift in endosomal/lysosomal pH are minor compared to those caused by iron-mediated probe quenching. This finding is in accordance with the recently published application of the fluorescein-based probe calcein-AM to monitor the lysosomal labile iron pool.[43]

Responsiveness to Clinical Iron Chelators. To evaluate potential application of the fluorescent probes in the diagnosis and evaluation of iron-related diseases, sensor responsiveness was tested against the clinical medications deferasirox (DFR) and deferiprone (DFP), both orally active iron chelators routinely used for iron excretion in iron-overloaded patients. The chelation potency of DFR and DFP was measured by **20** in BMMØ and is shown in comparison to the data obtained for DFO (Figure 8). On the basis of the individual pFe^{3+} values of all three chelators, the hexadentate iron chelator DFO (pFe^{3+} = 26.6) was expected to exhibit the most efficient iron chelation correlated with a high fluorescence signal of the sensor. However, DFO iron chelation is slowed by its membrane impermeability and endocytic uptake route. In contrast to DFO, DFR (pFe^{3+} = 22.5) benefits from high lipophilicity and low

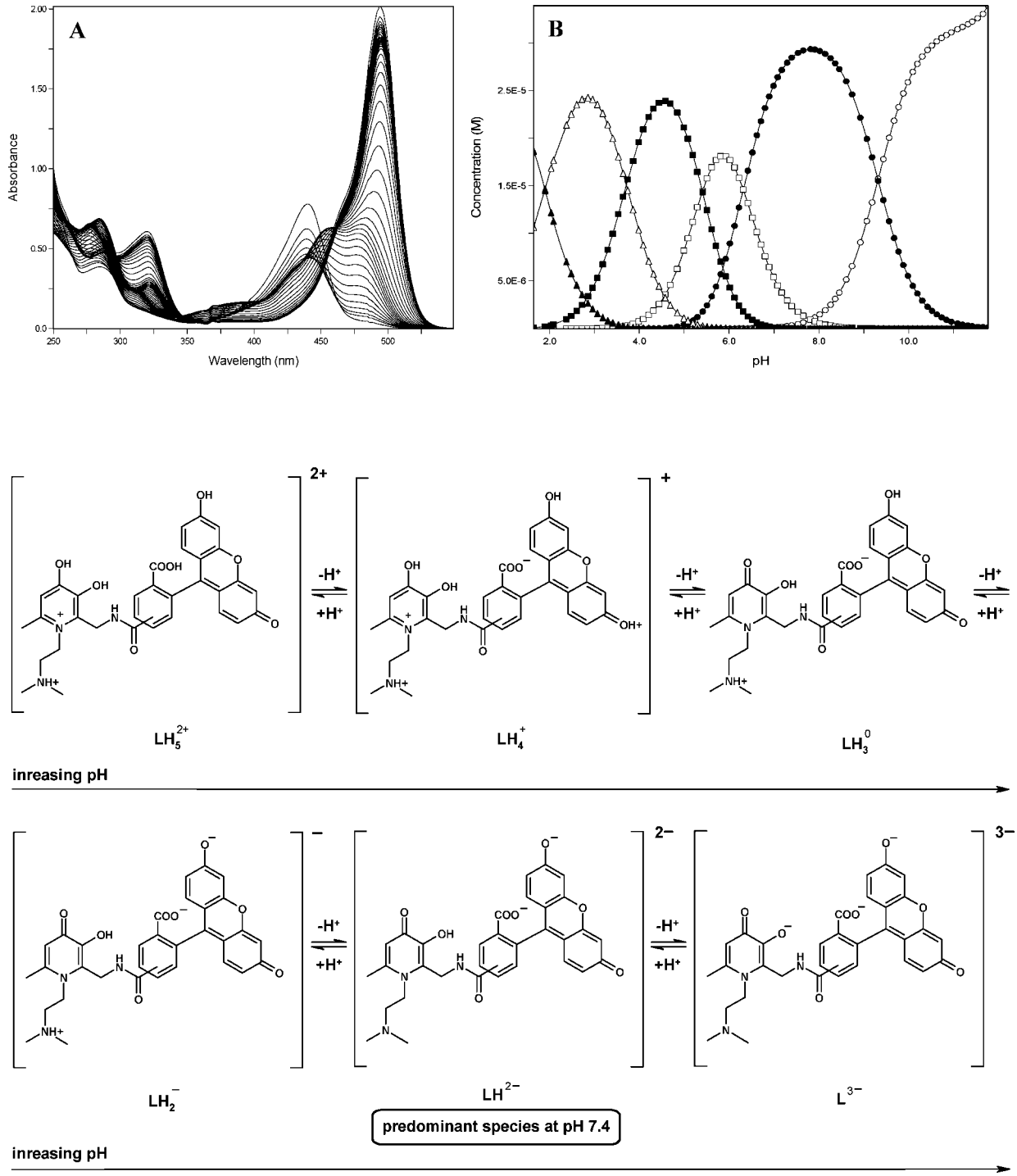

Figure 4. Spectrophotometric determination of the sensor solution properties: (A) pH dependent UV/vis spectra of **20** (34 μM) over the pH range of 1.65−11.16; (B) speciation plot of **20** (▲, LH_5^{2+}; △, LH_4^{+}; ■, LH_3^{0}; □, LH_2^{-}; ●, LH^{2-}; ○, L^{3-}).

molecular weight providing for rapid intracellular distribution and a higher chelation potency within the measured time range. Correspondingly, the tridentate chelator shows the largest **20** fluorescence increase (62.23%) after the initial 20 min incubation period followed by DFO (48.22%) in comparison to untreated **20**-stained cells set at 0%.

In contrast to DFO and DFR, **20** quenching was observed in the case of the bidentate chelator DFP ($pFe^{3+} = 19.5$, −7.21%). This effect is due to the applied staining procedure. As cells were pretreated with the chelators, subsequent fluorescent probe pulsing confronted the intracellular chelator−iron complexes with a huge excess of **20**. DFP and **20** both complex iron via an HPO based chelation unit and show comparable iron affinities. Confronted with a large **20** excess, intracellular DFP had no affinity advantage and consequently an iron exchange between the DFP−iron complex and the probe occurred, resulting in the observed quenching processes. In similar experiments applying **9**, cells were stained prior to application of the chelators. With this setup it could be shown that within the monitored incubation period DFP induced a clear 45% fluorescence recovery ranging between DFO (40%) and DFR (77%) in relation to untreated cells set at 0%.[42] It can therefore be concluded that in the case of DFP the observed **20** quenching is a methodical and not a biochemical effect.

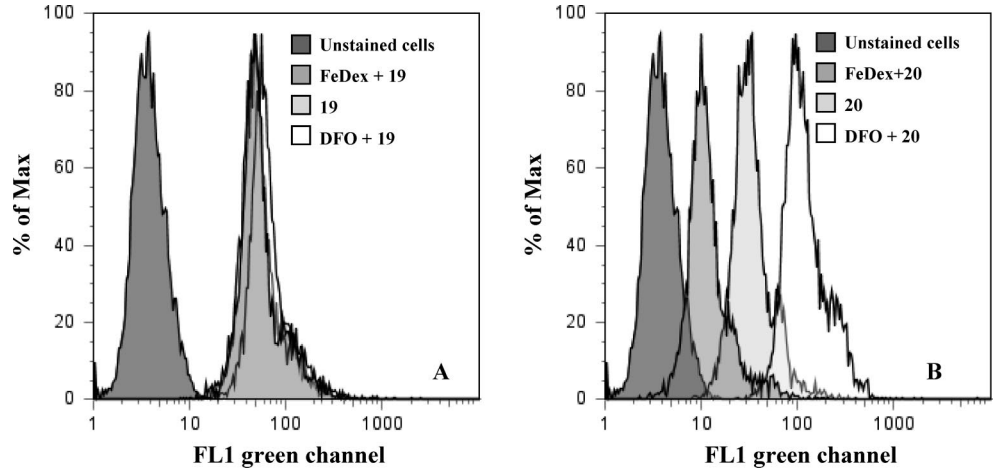

Figure 5. Representative flow cytometric histograms of the benzyl-protected iron-insensitive probe **18** (A) and its iron-sensitive analogue **20** (B) in response to changes of intralysosomal iron concentrations after 1 h. Data were acquired in the green Fl_1 channel. Gates were based on dot-plots of untreated cell populations. Macrophages were stained with the fluorescent compounds (5 μM) during a 20 min incubation period at 37 °C and 7.5% CO_2 in the dark and subsequently treated for 1 h with iron dextran (500 μg/mL) for iron saturation and DFO (1 mM) for iron depletion. Histograms of unstained cells are plotted in comparison to histograms of stained cells without treatment as well as after iron dextran and DFO treatment.

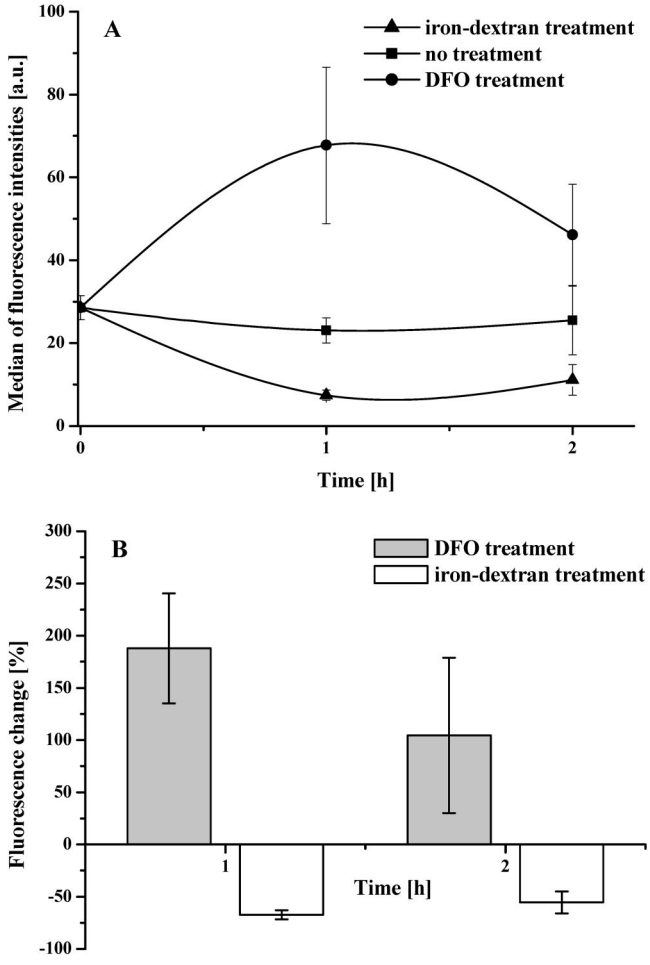

Figure 6. Intracellular fluorescence in BMM∅ labeled with **20** during a 2 h incubation period in response to endosomal/lysosomal iron supplementation using iron dextran (500 μg/mL) and lysosomal iron deprivation using DFO (1 mM) according to the procedure described in Figure 5. Kinetics of intracellular fluorescence (A) as well as percentage of fluorescence changes between untreated and treated cells (B) are shown as mean values ± SEM of triple FACS measurements.

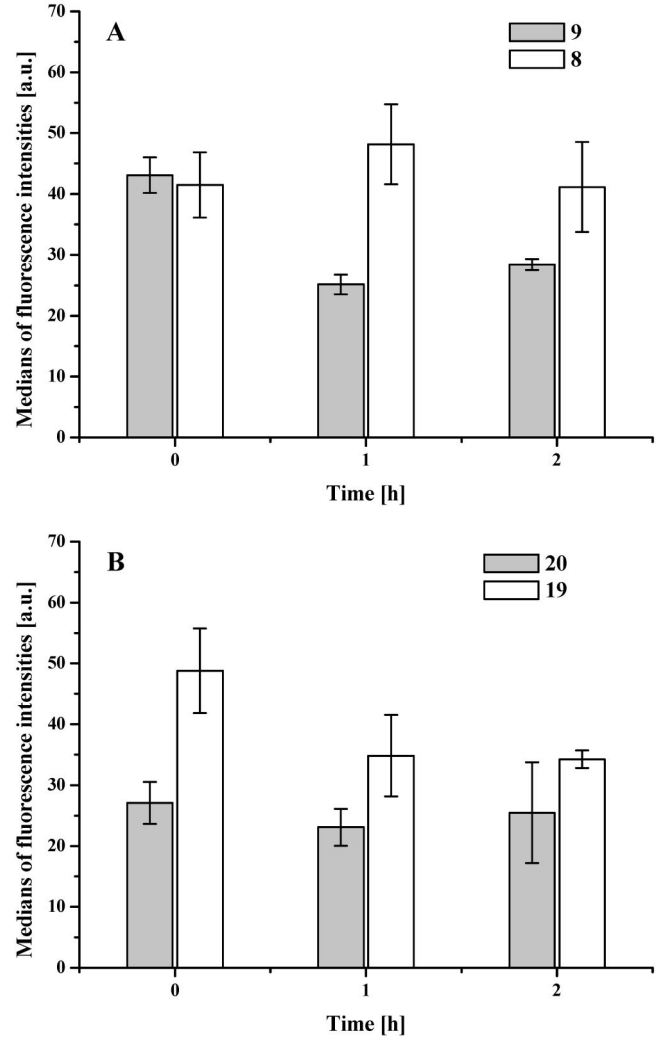

Figure 7. Comparative plots of untreated BMM∅ stained with the iron-sensitive sensors **9** (A)/**20** (B) and their corresponding iron-insensitive precursors **8/19** measured by FACS after probe loading for 20 min ($t = 0$) and at $t = 1$ and 2 h. Shown are median values ± SEM of triple measurements.

Intracellular Distribution Studies. In order to characterize the intracellular fate of the iron-sensitive probes, bone marrow derived macrophages were incubated with 75 μM probe solutions in iron-free PBS for 20 min. Because of the negatively

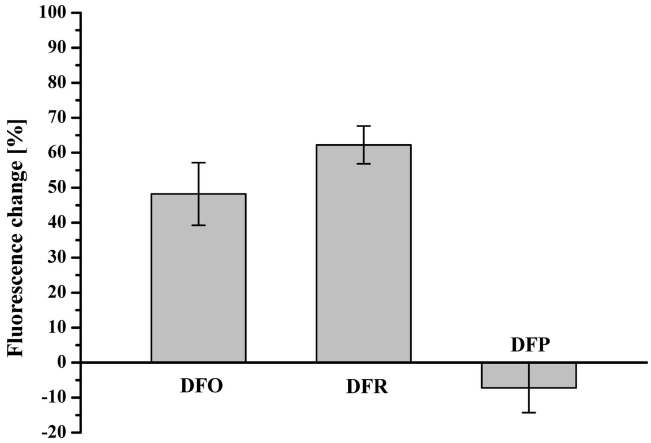

Figure 8. Responsiveness of intracellular **20** fluorescence to clinically approved iron chelators. BMMØ was treated for 40 min with DFO (100 μM), DFR (100 μM), and DFP (100 μM) and subsequently stained with **20** for 20 min at 37 °C and 7.5% CO_2. Fluorescence was measured by FACS as described in Figure 5. Shown are median values ± SEM of triplicate measurements.

charged nature of both probes at physiological pH, their intracellular localization, i.e., trafficking, accumulation, and distribution, is expected to be confined to the endosomal/lysosomal system. Preliminary confocal microscopy analysis of **9**-labeled cells revealed a distinct vesicular localization of the probe 20 min after loading, most likely representing endosomal/lysosomal compartments.[35]

A similar localization within intracellular vesicles was observed for **20**. Illustrated in Figure 9 are confocal microscopy images of **20**-labeled cells acquired after a 20 min pulse with **20** and a subsequent chase over a 60 min period, initially in the presence of DFO and its subsequent replacement with iron dextran. As shown in Figure 9A, a 20 min incubation period resulted in efficient probe saturation for most of the macrophages. Extracellular probe sticking to outer cell membranes indicates that cells are still in the process of probe uptake, which possibly represents a preliminary stage to endocytic probe internalization. On the other hand, images acquired later in the 60 min chase period illustrate completed cellular probe uptake and reveal a defined vesicular probe localization (Figure 9B−D) as observed for **9**.

To verify functionality of vesicular **20**, fluorescence intensity was measured in response to DFO treatment for 20 and 40 min during the chase period. Considerable fluorescence recovery in probe loaded vesicles could be observed upon incubation with DFO, showing equilibrated dequenching conditions after a 20 min incubation period with no notable increase after 40 min (Figure 9B,C). Cross-check of sensor responsiveness by subsequent application of iron dextran for an additional 20 min incubation period to the DFO treated macrophages resulted in significant intracellular fluorescence decrease as excessive exogenous iron quenched the fluorescent sensor (Figure 9D).

To characterize the intracellular compartments accumulating the probes, colocalization studies using Texas Red labeled dextran (DexTR) as a lysosomal tracer were carried out in **20**-labeled macrophages. The representative colocalization pattern acquired after the initial 20 min probe incubation period is illustrated in Figure 10A−C and shows a direct comparison of cellular fluorescence recorded in the green and red channels. At this early time point after loading, **20** was only present within DexTR negative compartments most likely representing early endosomes as shown in magnification in Figure 10E. Subsequent monitoring of **20** localization over a 30 min chase period revealed progressive probe trafficking to DexTR positive compartments (Figure 10F−T) and complete absence of the probe from DexTR negative compartments after 30 min of chase (Figure 10T), consistent with the dynamics of endocytic pathways. Overall probe fluorescence intensity over the 30 min incubation period was not affected (Figure 10A,F,K,P).

Studies applying DexTR-labeled cells treated with DFO or iron dextran and subsequently labeled with **20** allowed combinatorial monitoring of sensor responsiveness and lysosomal colocalization. Illustrated in Figure 11A−C are representative magnifications of macrophages measured in the green and red channels after a 60 min incubation period. At this later time point **20** fluorescence colocalized predominantly with DexTR labeled late endosomes/lysosomes. DFO-treated cells exhibited considerably brighter **20** fluorescence, suggesting significant intracellular probe dequenching by this iron chelator. Iron dextran treated cells illustrated in Figure 11I−K show the same colocalization pattern in combination with a reduced **20** fluorescence signal following vesicular probe quenching.

Further characterization of cellular sensor location was carried out in macrophages stained for endosomes, endoplasmic reticulum, and mitochondria, using DexTR, ER-Tracker Red, and MitoTracker Deep Red, respectively. Mixed solutions of tracer and **20** were applied to cells for 20 min. At this early time point, DexTR and **20** are predicted to locate to endosomes, whereas lysosomes are expected to be tracer- and sensor-free. As illustrated in Figure 12A−E, there is partial colocalization between the sensor and DexTR; however, DexTR-negative **20**-containing vesicles and DexTR-positive **20**-negative vesicles are also present. These findings suggest partially divergent uptake pathways for DexTR and **20**. ER-labeling (Figure 12F−J) and mitochondrial labeling (Figure 12K−O) reveal characteristic staining of these organelles and no colocalization with the iron sensor, confirming the sensor confinement to the endocytic pathways.

Probe Uptake. To further specify endocytic probe uptake mechanisms, bone marrow derived macrophages were treated with cytochalasin D, a commonly used inhibitor of actin-dependent macropinocytosis. The cells were incubated with cytochalasin D for 30 min and subsequently treated with **20** or DexTR (10 kDa) for 20 min. Confocal microscopy revealed a reduction in DexTR uptake, whereas uptake of **20** was not affected (data not shown), suggesting that in contrast to DexTR, **20** is engulfed by actin-independent pinocytosis.

Conclusions

Lysosomes have been suggested to play a major role in the intracellular regulation and homeostasis of iron metabolism. Because of the breakdown of iron-containing endocytosed as well as autophagocytosed material, significant concentrations of labile iron accumulate in the lysosomes, potentially catalyzing organelle rupture and subsequent cell death. To study lysosomal iron and its influence on cellular iron homeostasis, we have synthesized the novel fluorescein-labeled iron(III) chemosensors **9** and **20** featuring substituted 3-hydroxypyridin-4-one (HPO) based chelation moieties specifically targeting the endosomal/lysosomal system for iron monitoring. Detection of cellular quenching and dequenching processes showed a clear difference in sensor responsiveness to manipulations of intracellular iron concentrations, with **20** being of magnitudes more responsive. Because pK_a values give no indication of differences in iron binding properties of both probes, substitution in the 1-position of **20** is most likely responsible for the observed differences.

Owing to the deprotonated fluorescein moiety, both probes are highly hydrophilic and virtually membrane impermeable at

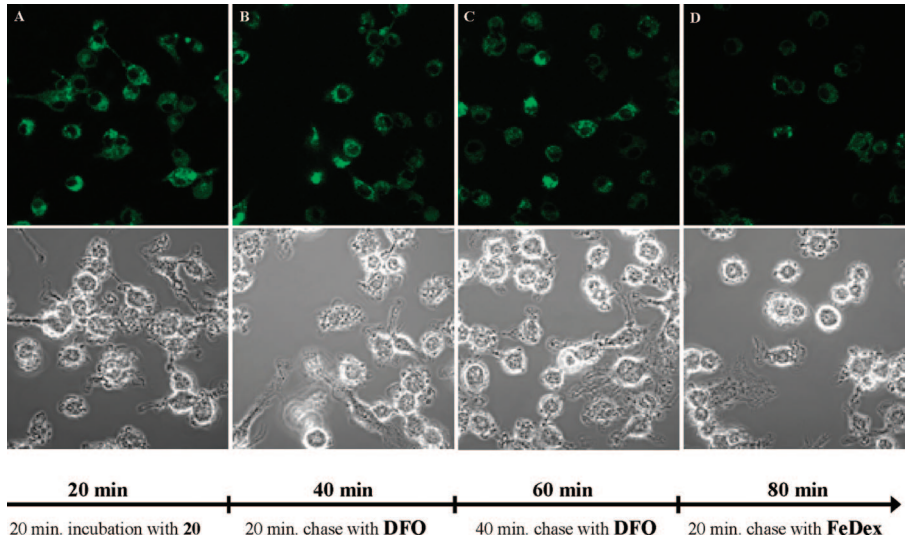

Figure 9. Representative confocal microscopy images of the sensor distribution in BMMØ. Cells were cultured on μ-channel slides and treated with a 75 μM solution of **20** for 20 min. Fluorescence was excited at a 488 nm excitation wavelength using a 505 nm long-pass filter for emission. Fluorescence data are shown in comparison to the corresponding bright field images. Untreated **20**-labeled cells were monitored after the initial 20 min incubation period (A). Following exchange of the incubation buffer with a 1 mM DFO solution, cells were monitored after an additional 20 min (B) and 40 min (C) incubation period. Subsequent application of a 500 μg/mL solution of iron dextran (FeDex) was measured after a further 20 min (D).

physiological pH. Correspondingly, cellular imaging experiments using confocal microscopy in macrophages revealed compartmentation of both probes in endosomal/lysosomal compartments due to a pinocytic uptake route. Furthermore, application of iron(III) insensitive precursors could demonstrate that endosomal maturation accompanied by acidification did not influence iron related measurements. Correspondingly, the probes proved to be highly sensitive and reproducible in assessing the chelation potency of the clinically employed chelators, deferiprone, desferrioxamine, and deferasirox. Development of fluorescein coupled HPO-based iron(III) sensors therefore represents a considerable step forward toward developing techniques to study subcellular iron distribution. Combination of exclusive endosomal/lysosomal accumulation with the high HPO iron specificity/affinity and reproducibly high responsiveness toward intracellular changes of free iron resulted in a promising class of new sensors to study iron metabolism under physiological and pathophysiological conditions. Application of these probes in real-time monitoring of the endosomal/lysosomal labile iron pool will allow assessment of iron status in patients under iron supplementation or chelation therapy. These novel diagnostic tools will also provide valuable insights into the role of intracellular trafficking and homeostasis of redox-active labile iron for diseases as diverse as infections, autoimmunity, and cancer. They will significantly contribute to a facilitated development of more efficient iron chelating agents.

Experimental Section

Cell Culture and Reagents. Bone marrow derived macrophages (BMMØ)were isolated from the femurs and tibias of 6−8 month old C57BL/6 mice (Harlan Bioproducts, Bicester, U.K.) according to standardized procedures. Cells were plated in Dulbecco's modified Eagles medium (DMEM) supplemented with 10% heat-inactivated fetal calf serum (FCS), 5% horse serum, 1% L-glutamine, and 20% L929 cell culture supernatant as a source of macrophage colony-stimulating factor (M-CSF; Biochrome, Berlin, Germany). Cells were cultivated at 37 °C and 7.5% CO_2. Mature adherent macrophages were harvested after 7 days of culture and stored at −80 °C in 10% DMSO to be replated when required. Thawed cells were cultured overnight, and nonadherent cells were washed off prior to manipulations. No antibiotics were used in the culture medium.

Manipulation of the intracellular iron content was carried out by iron supplementation or deprivation treatments. Cells were incubated for up to 2 h prior to staining in 500 μg/mL iron dextran (Pharmacosmos A/S, Holbaek, Denmark) for cellular iron overloading and in 1 mM/100 μM deferoxamine mesylate (DFO, Sigma Aldrich, Gillingham, U.K.), 100 μM deferiprone (DFP, Sigma Aldrich, Gillingham, U.K.), or deferasirox (DFR) for iron deprivation.

Inhibition of macropinocytosis by cytochalasin D (Calbiochem Merck Chemicals, Nottingham, U.K.) was performed as follows. Cytochalasin D was provided as a 1 mg/mL stock solution in DMSO and diluted with iron-free PBS to a 10 μg/mL solution. BMMØ was incubated with the compound for 30 min, washed with Chelex-treated PBS, and subsequently treated with a 75 μM solution of the fluorescent iron sensor or a 100 μg/mL solution of DexTR (Molecular Probes Invitrogen, Paisley, U.K.).

Flow Cytometry. For flow cytometric measurements nonadherent cells were washed off from cultivated cell monolayers, which were subsequently incubated at 4 °C for 20 min in cold PBS (pH 7.4) treated with Chelex-100 (sodium form, Sigma Aldrich) to remove iron contaminations. The cells were harvested, washed three times with cold iron-free PBS, and split into FACS tubes at 10^5 cells per tube. All subsequent washes and procedures were carried out on ice unless otherwise stated. The cells were incubated with the fluorescent probes, provided as 10 mM stock solutions in DMSO and diluted with cold iron-free PBS at a final concentration of 5 μM, for 20 min at 37 °C and 7.5% CO_2. Cells were washed and resuspended in cold Chelex-treated PBS. Measurements were carried out on a FACSCalibur flow cytometer (BD Biosciences), and analysis proceeded via CellQuest and FlowJo softwares. Gates were based on dot-plots of untreated cell populations. Medians of at least 10 000 events were recorded and corrected for cell autofluorescence. Mean values were calculated from three independent experiments.

Confocal Microscopy. Confocal microscopic imaging of intracellular probe distribution was carried out using BMMØ plated onto uncoated μ-channel slides (Ibidi, Munich, Germany) at 10^5 cells per slide. For lysosomal colocalization experiments, cells were cultured with 100 μg/mL DextranTR (10 kDa) for 4 h and chased overnight. The cells on the μ-channel slide were washed three times with 600 μL portions of Chelex-treated PBS

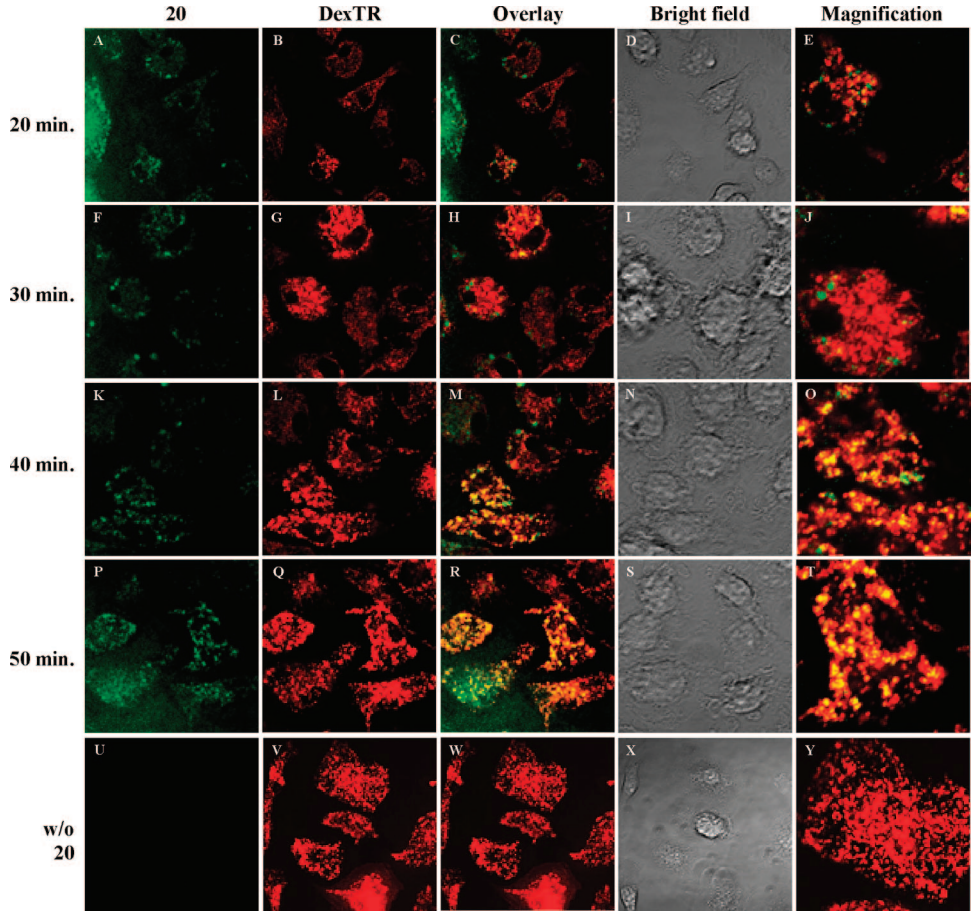

Figure 10. Representative confocal microscopy images of intracellular colocalization studies of **20** in BMMØ with dextran Texas Red labeled lysosomes. Cells were cultured on μ-channel slides, treated with a 100 μg/mL dextran Texas Red solution for 4 h, and chased overnight. Dextran Texas Red labeled cells were stained for 20 min with a 75 μM solution of **20**, followed by subsequent exchange of the incubation solution with iron-free PBS. Intracellular fluorescence of stained cells was excited at 543 nm (dextran texas red) or at 488 nm (**20**) using a 560 and a 505 nm long-pass filter for emission. Fluorescence of stained cells was measured in the green (A, F, K, P) as well as in the red (B, G, L, Q) channel, and data were merged for evaluation of colocalization in yellow (C, H, M, R). Fluorescence data are shown in comparison to the corresponding bright field images (D, I, N, S). Magnifications of merged fluorescence data show detailed changes in localization of the probe with respect to the tracer at various stages of cellular probe uptake (E, J, O, T). Parts A−E were taken immediately after probe loading. Parts F−J were taken after a 10 min chase. Parts K−O were taken after a 20 min chase. Parts P−T were taken after a 30 min chase. Parts U−X are BMMØ labeled with dextran Texas Red only as a control for the broad emission spectrum of the red channel.

to remove cell culture medium and incubated for 20 min with a 75 μM probe solution in iron-free PBS at 37 °C and 7.5% CO_2. For endosomal, mitochondrial, and endoplasmic reticulum colocalization experiments, 100 μg/mL DextranTR, 1 μM ER-Tracker Red (Invitrogen, Paisley, U.K.), or 250 μM MitoTracker Deep Red (Invitrogen, Paisley, U.K.) was added to a 100 μM probe solution in iron-free PBS and applied to cells for 20 min at 37 °C and 7.5% CO_2. The cells were repeatedly washed with iron-free PBS and kept on ice for subsequent measurements or at 37 °C for probe chasing. Fluorescence was measured using an inverted Zeiss confocal fluorescent microscope using a 63× oil immersion objective. Images were acquired and analyzed by Zeiss LSM image browser software.

Physical Measurements. Optical characterization of the fluorescent probes **9** and **20** was performed on a Perkin-Elmer spectrophotometer type UV/vis Lamda2S and a Perkin-Elmer spectrofluorometer type LS 50B.

^{1}H NMR spectra were recorded using a Bruker 360 MHz NMR spectrometer. Chemical shifts δ are reported in ppm.

Mass spectra (ESI) analyses were carried out by the Mass Spectrometry Facility, School of Health and Life Sciences, 150 Stamford Street London SE1 9NH, U.K.

For pK_a determinations, an automatic titration system comprising an autoburet (Metrohm Dosimat 765, 1 mL syringe) and a Mettler Toledo MP230 pH meter with a Metrohm pH electrode (6.0133.100) and a reference electrode (6.0733.100) was used. A 0.1 M KCl electrolyte solution was used to maintain the ionic strength. For the measurements the temperature of the probe solution was maintained in a thermostatic jacketed titration vessel at 25 ± 0.1 °C using a Techne TE-8J temperature controller. The solution was stirred vigorously during the experiment. A Gilson Mini-plus#3 pump with speed capability (20 mL/min) was used to circulate the probe solution through a Hellem quartz flow cuvette. A cuvette path length of 10 mm was used and the flow cuvette mounted on a HP 8453 UV−visible spectrophotometer. All instruments were interfaced to a computer and controlled by a Visual Basic program. The pH of the probe solution was increased by 0.1 pH unit by the addition of KOH from the autoburet. When pH readings varied by <0.001 pH unit over a 3 s period, an incubation period of 1 min was adopted. At the end of the equilibrium period, the spectrum of the solution was recorded. The cycle was repeated automatically until the defined end point pH value was achieved. Titration data were analyzed by pHab.[44]

pK_a Determination. The pH electrodes were calibrated by titrating a volumetric standard strong acid HCl (0.15 mL, 0.2092 M) in KCl (15 mL, 0.1 M) with KOH (0.1 M) under an argon atmosphere at 25 °C. The E_0, slope of the electrode, and pK_w of the solution were both optimized by GLEE.[45] Following electrode calibration, a 34 μM solution of **20** in 11.162 mL of 0.1 M KCl at an initial pH value of 1.646 were alkalimetrically titrated to pH

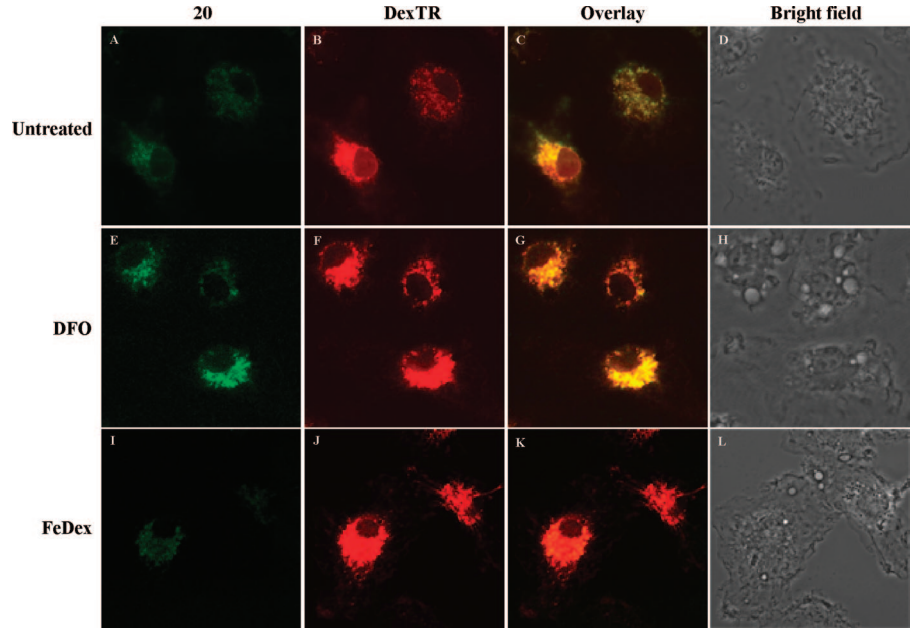

Figure 11. Representative confocal microscopy images of intracellular colocalization studies of **20** in BMMØ using dextran Texas Red labeled lysosomes. Colocalization studies according to the experimental setup described in Figure 10 were carried out in DFO (E, F) and iron dextran (I, J) pretreated cells as well as untreated cells (A, B), with 1 h of incubation with 75 μM **20**. Findings are illustrated together with merged fluorescence data showing a high degree of lysosomal colocalization in yellow at a later stage of cellular probe processing (C, G, K). Fluorescence data are shown in comparison to the corresponding bright field images (D, H, L).

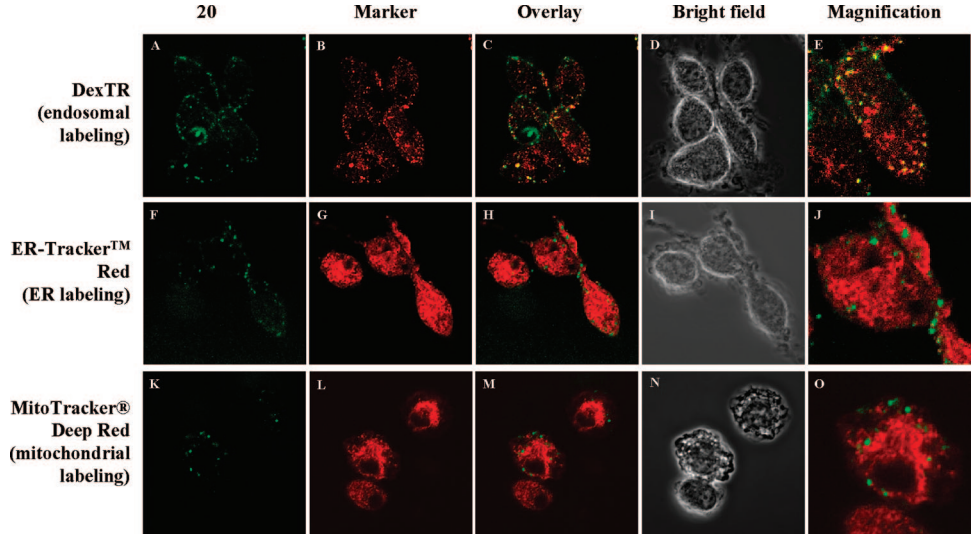

Figure 12. Representative confocal microscopy images of intracellular colocalization studies of **20** in BMMØ with dextran Texas Red labeled endosomes (A−E), ER-Tracker labeled endoplasmic reticulum (F−J) and MitoTracker labeled mitochondria (K−O). Cells were treated simultaneously with 100 μM **20** and 100 μg/mL dextran Texas Red, 1 μM ER-Tracker Red for 20 min, or 250 μM MitoTracker Deep Red, followed by subsequent exchange of the incubation solution with iron-free PBS. Fluorescence data were collected as described in Figure 10. Green (A, F, K) and red (B, G, L) fluorescence data were merged together (C, H, M) to represent colocalization in yellow, also in detail in magnifications (E, J, O). Fluorescence data are shown in comparison to the corresponding bright field images (D, I, N).

11.162. The spectra of **20** and the titration experimental data at different pH values were analyzed by refining the extinction coefficients of the protonated and deprotonated species.

log *P* Determination. The log *P* values of **9** and **20** were determined by the shake-flask method using a *n*-octanol−aqueous buffer system at 25 °C. Because the log *P* is strictly defined for neutral molecules, the partition of both probes was measured in citric acid buffer at pH 3 and pH 4.5, respectively, providing experimental conditions where according to probe speciation the neutral LH_3 species predominates. The absorbance of a buffered probe solution of known concentration was recorded spectrophotometrically, and different ratios of buffered probe solution and *n*-octanol were then shaken by vigorous stirring for 1 h. The stirring interval was repeated three times, and the layers were subsequently separated by centrifugation at 25 °C. The aqueous phases were again measured spectrophotometrically showing a decrease of probe absorbance due to partition into the organic phase. Lipophilicity, directly correlating with the detected decrease in probe absorbance, was derived from the recorded UV spectra according to the following equation:

$$P = \frac{(A_0 - A_1)V_{aq}}{A_1 V_o}$$

where A_0 is the initial absorbance of the aqueous phase, A_1 is the absorbance of the aqueous phase after separation of the aqueous

phase by centrifugation, V_{aq} is the total volume of the aqueous phase, and V_o is the total volume of the organic phase.

Syntheses. All starting materials were obtained from commercial sources and used without further purification. 3-Hydroxy-2-methyl-4*H*-pyran-4-one (maltol, **1**) was purchased from Cultor Food Science, and 5-hydroxy-2-(hydroxymethyl)-4*H*-pyran-4-one (kojic acid, **10**) and 5(6)-carboxy fluorescein **6** were purchased from Fluka. Syntheses of **2**−**5** and **11**−**14** were based on procedures described previously.[28] Because of the applied mix of isomers of 5(6)-carboxy fluorescein, no NMR data were recorded for **9** and **20** and compound identity was established on the basis of mass spectrometry measurements.

3-Methoxy-2-methyl-4*H*-pyran-4-one (2). A solution of 63.06 g (500 mmol) maltol in 300 mL of 10% potassium hydroxide solution was cooled to 0 °C in an ice/water bath. An amount of 52.04 mL (69.37 g, 550 mmol) of dimethyl sulfate was added dropwise to the solution, which was kept at 0 °C throughout the reaction. Stirring continued for 4 h and was followed by extraction of the reaction solution with dichloromethane (3 × 100 mL). The combined organic extracts were washed with 5% KOH solution and water (3 × 100 mL), dried over sodium sulfate, and filtered. The solvent was removed in vacuum to yield the product as an orange oil (49.85 g, 356 mmol, 71%). ^{1}H NMR ($CDCl_3$) δ: 2.34 (s, 3H), 3.86 (s, 3H), 6.36 (d, 1H), 7.66 (d, 1H). *m*/*z*: 141 (M + 1)$^+$.

3-Methoxy-2-methylpyridin-4(1*H*)-one (3). To a solution of 10.51 g (75 mmol) **2** in 80 mL of water were added 10 mL portions of aqueous ammonia solution under reflux at 60 °C until all starting material had completely reacted. Subsequently, the excess ammonia was evaporated under reduced pressure and the aqueous reaction solution dried in high vacuum. The solid brown residue was thoroughly resuspended and washed in acetone, filtered, and dried to yield the product as a light-brown solid (8.15 g, 59 mmol, 78%). ^{1}H NMR ($CDCl_3$) δ: 2.43 (s, 3H), 3.80 (s, 3H), 6.47 (d, 1H), 7.56 (d, 1H). *m*/*z*: 140 (M + 1)$^+$.

5-{[Benzyl(methyl)amino]methyl}-3-methoxy-2-methyl-pyridin-4(1*H*)-one (4). In 120 mL of ethanol, an amount of 46.46 mL (43.62 g, 360 mmol) of *N*-benzylmethylamine was mixed with 14.62 mL (5.41 g, 180 mmol) of a 37% aqueous formaldehyde solution and stirred at room temperature for 30 min. An amount of 8.35 g (60 mmol) of **3** was added, and the brown solution was boiled under reflux until the reaction was complete. The solvent was removed under reduced pressure, and the resulting brown oil was additionally dried in high vacuum. The viscous residue was covered with acetone and left at 4 °C overnight to allow crystallization of the product. The resulting precipitate was extensively washed with acetone, filtered, and dried in high vacuum to yield **4** as a white solid (14.22 g, 52 mmol, 87%). ^{1}H NMR (DMSO-d_6) δ: 2.09 (s, 3H), 2.19 (s, 3H), 3.34 (s, 2H), 3.50 (s, 2H), 7.27 (m, 5H), 7.49 (s, 1H). *m*/*z*: 273 (M + 1)$^+$.

3-Methoxy-2-methyl-5-[(methylamino)methyl]pyridin-4(1*H*)-one (5). An amount of 5.45 g (20 mmol) of **4** was dissolved in 100 mL of ethanol in a hydrogenolysis flask and debenzylated overnight via hydrogenolysis in the presence of a 10% Pd/C catalyst. The catalyst was subsequently filtered off and the solvent removed under reduced pressure. The residual viscous brown oil was covered with dichloromethane and kept at 4 °C overnight to allow crystallization of the product. The resulting solid was filtered off and the filtrate stored at 4 °C to be used in several corresponding cycles of precipitation until the formed product was completely collected. The combined precipitates were extensively washed with dichloromethane, filtered, and dried in high vacuum to yield **5** as a white solid (3.46 g, 19 mmol, 95%). ^{1}H NMR (D_2O) δ: 2.24 (s, 3H), 2.46 (s, 3H), 3.63 (s, 3H), 3.79 (s, 2H), 7.64 (s, 1H). *m*/*z*: 183 (M + 1)$^+$.

4(and 5)-[(3-Methoxy-2-methyl-4-oxopyridin-5-yl)(methylamino)methylcarbamoyl]-2-(3-hydroxy-6-oxo-6*H*-xanthen-9-yl)benzoic acid (8). To a solution of 500 mg (1.33 mmol) of 5(6)-carboxyfluorescein (**6**) in 15 mL of DMF were added 329 mg (1.59 mmol) of dicyclohexylcarbodiimide (DCCI) and 183 mg (1.59 mmol, 1.2 equiv) of *N*-hydroxysuccinimde. The reaction solution was stirred at room temperature overnight in the dark to complete the intermediate formation of the activated fluorophor **7**. Subsequently, the formed white *N*,*N*-dicyclohexylurea (DCU) precipitate was filtered off and an amount of 266 mg (1,46 mmol) of **5** was added to the red filtrate. The mixture was stirred at room temperature for 24 h in the dark, followed by solvent removal under reduced pressure. The orange residue was taken up in 25 mL of 1.25% sodium hydroxide solution and the aqueous layer washed successively with chloroform (3 × 10 mL). The pH of the aqueous reaction solution was adjusted with 4 N hydrochloric acid to pH 3, resulting in the formation of a thick orange precipitate. After completion of the precipitation the orange solid was filtered off and dried under high vacuum. Purification of the crude product was conducted by preparative HPLC methods using a reversed phase C_{18} column and application of an isocratic water/0.1% TFA (buffer A) and acetonitrile (buffer B) gradient (432 mg, 0.80 mmol, 60%). *m*/*z*: 563 (M + Na^+).

4(and 5)-[(3-Hydroxy-2-methyl-4-oxopyridin-5-yl)(methylamino)methylcarbamoyl]-2-(3-hydroxy-6-oxo-6*H*-xanthen-9-yl)benzoic acid (9). A suspension of 100 mg (0.19 mmol) **8** in 5 mL of anhydrous dichloromethane was flushed with nitrogen and cooled to 0 °C in an ice/water bath. An amount of 2 mL of BCl_3 solution (1 M in dichloromethane) was added dropwise to the cooled solution, and the mixture was stirred at room temperature in the dark until complete conversion of the starting material. An amount of 10 mL of methanol was added, and the mixture was stirred for 30 min to eliminate excess of BCl_3. The solvent was removed under reduced pressure, and after additional drying of the residue in high vacuum the crude product was purified by recrystallization. Dissolution of the solid in a minimal amount of methanol and subsequent precipitation with excess acetone yielded the pure yellow hydrochloride salt of the fluorescent product as an amorphous powder. Purity of the compound was verified by HPLC using a reversed phase C_{18} column and applying an isocratic water/0.1% TFA (buffer A) and acetonitrile (buffer B) method (for data, see Supporting Information) (25 mg, 0.04 mmol, 23%). *m*/*z*: 527 (M + 1)$^+$.

2-(Chloromethyl)-5-hydroxy-4(1*H*)-pyran-4-one (11). A solution of 4.97 g (35 mmol) of 2-hydroxymethyl-5-hydroxypyrone (**10**, kojic acid) in 20 mL of distilled thionyl chloride was allowed to stir for 1 h at room temperature. Precipitation of the crude product in the form of a brownish powder occurred, which was collected by filtration and washed with petrol ether to furnish **11** as a white amorphous solid (4.50, 28 mmol, 80%). ^{1}H NMR (DMSO-d_6) δ: 4.66 (s, 2H), 6.57 (s, 1H), 8.13 (s, 1H). *m*/*z*: 161 (M + 1)$^+$.

5-Hydroxy-2-methyl-4(1*H*)-pyran-4-one (12). In a three-neck round-bottom flask fitted with reflux condenser and thermometer, an amount of 10.44 g (65 mmol, 1 equiv) of **11** was suspended in 50 mL of water and heated to 50 °C. Under vigorous stirring, an amount of 8.52 g (130.34 mmol, 2 equiv) of zinc powder was slowly added to the suspension while maintaining a constant reaction temperature of 50 °C. The reaction solution was subsequently heated to 70 °C and a total of 19.5 mL of concentrated hydrochloric acid was added dropwise keeping the reaction temperature between 70 and 80 °C. Stirring continued for another 3 h at 70 °C, and excess of zinc powder was immediately removed by filtration of the hot reaction solution. The cooled filtrate was extracted with dichloromethane (3 × 50 mL), and the combined organic extracts were dried over sodium sulfate and filtered. The solvent was removed under reduced pressure to yield **12** as a white powder (6.29 g, 50 mmol, 77%). ^{1}H NMR (DMSO-d_6) δ: 2.23 (s, 3H), 6.23 (s, 1H), 7.96 (s, 1H), 8.98 (s, 1H). *m*/*z*: 127 (M + 1)$^+$.

3-Hydroxy-2-(hydroxymethyl)-6-methyl-4*H*-pyran-4-one (13). An amount of 15.13 g (120 mmol) of **12** was dissolved in 120 mL of an aqueous 1.1 M sodium hydroxide solution and stirred at room temperature for 5 min. After dropwise addition of 10.22 mL (3.78 g, 126 mmol) of formaldehyde solution (37% in water), the mixture was stirred for 24 h and subsequently the pH of the solution was adjusted with concentrated hydrochloric acid to pH 1. The formation of a thick white precipitate occurred, which was kept at 4 °C overnight to ensure complete product precipitation.

The solid was filtered off, washed with cold ether, and dried in high vacuum to yield **13** as a white crystalline powder (14.76 g, 95 mmol, 79%). ^{1}H NMR (DMSO-d_6) δ: 2.26 (s, 3H), 4.39 (s, 2H), 6.22 (s, 1H), 8.88 (br s, 1H). *m/z*: 157 $(M + 1)^+$.

3-(Benzyloxy)-2-(hydroxymethyl)-6-methyl-4*H*-pyran-4-one (14). To a solution of 15.61 g (100 mmol) of **13** in methanol was added a total of 10 mL of a 11 M aqueous sodium hydroxide solution, and the mixture was heated to reflux. An amount of 12.66 mL (13.92 g, 110 mmol, 1.1 equiv) of benzyl chloride was added dropwise to the solution, and the mixture was refluxed overnight. The NaCl precipitate was removed by filtration, and the solvent evaporated under reduced pressure. The brown viscose residue was taken up in dichloromethane and washed with 5% aqueous sodium hydroxide solution and water. The mixture was dried over soldium sulfate and filtered, and the solvent was evaporated under reduced pressure. Recrystallization of the crude product followed dissolution of the residue in a minimal amount of dichloromethane and the addition of an excess of petrolether. After filtration and drying of the precipitate the product was obtained as a white powder (15.36 g, 62 mmol, 62%). ^{1}H NMR ($CDCl_3$) δ: 2.24 (s, 3H), 4.31 (s, 2H), 5.16 (s, 2H), 6.22 (s, 1H), 7.34 (m, 5H). *m/z*: 247 $(M + 1)^+$.

3-(Benzyloxy)-1-[2-(dimethylamino)ethyl]-2-(hydroxy methyl)-6-methylpyridin-4(1*H*)-one (16). An amount of 7.39 g (30 mmol) of **14** was dissolved in 120 mL of dichloromethane. To the solution were added 5.47 mL (5.05 g, 60 mmol) of 3,4-dihydro-2*H*-pyran and a catalytic amount of *p*-toluenesulfonic acid (90 mg). The mixture was stirred at room temperature for 6 h and subsequently was washed with 5% sodium hydroxide solution and water (3 × 40 mL). After solvent evaporated under reduced pressure, **15** was yielded as a colorless oil and reacted in the next step without further purification. The tetrahydropyrane protected intermediate was taken up in 130 mL of water and 20 mL of ethanol. An amount of 9.88 mL (7.93 g, 90 mmol) of *N*,*N*-dimethylethylenediamine was added dropwise to the solution, and the mixture was heated to reflux until **15** had completely reacted. The solvent was removed under reduced pressure, and the residual brown oil dissolved in 60 mL of ethanol. The solution was adjusted to pH 1 using concentrated hydrochloric acid and further refluxed for 5 h. After evaporation of the solvent the dry residue was dissolved in 160 mL of water and extensively washed with diethyl ether (3 × 70 mL). The pH of the aqueous solution was adjusted to pH 12 using 10 M sodium hydroxide solution and extracted with dichloromethane (5 × 50 mL). The combined organic extracts were dried over sodium sulfate, filtered, and dried in vacuum to yield the crude product as a light-brown powder. Purification of **16** was carried out by column chromatography on silica gel (eluent, chloroform/methanol, 15:1 v/v) and furnished a white amorphous powder (3.99 g, 13 mmol, 42%). ^{1}H NMR ($CDCl_3$) δ: 2.22 (s, 6H), 2.27 (s, 3H), 2.51 (t, 2H), 4.08 (t, 2H), 5.15 (s, 2H), 6.32 (s, 1H), 7.34 (m, 5H). *m/z*: 317 $(M + 1)^+$.

3-(Benzyloxy)-1-[2-(dimethylamino)ethyl]-6-methyl-2-phthalimidomethyl-pyridin-4(1*H*)-one (17). An amount of 3.15 g (12 mmol) of triphenylphosphine was dissolved in 50 mL of tetrahydrofurane followed by 1.77 mg (12 mmol) of phthalimide. Subsequently, an amount of 3.16 g (10 mmol) of **16** was added and the resulting suspension was cooled to 0 °C in an ice/water bath. An amount of 2.36 mL (2.43 g, 12 mmol) of diisopropyl azodicarboxylate was added slowly to the suspension, and the mixture was stirred overnight at room temperature. The thin white precipitate formed after complete reaction of **16** was spinned down in a centrifuge, and the brown supernatant containing the product was additionally filtered through a syringe filter. The solvent was evaporated under reduced pressure to yield the crude product as a brown solid. Purification of **17** was carried out by column chromatography on silica gel (eluent, chloroform/methanol, 30:1) and furnished a white amorphous powder (1.02 g, 2.28 mmol, 23%). ^{1}H NMR ($CDCl_3$) δ: 2.16 (s, 6H), 2.38 (s, 3H), 3.47 (s, 2H), 4.23 (t, 2H), 4.72 (br s, sH), 5.38 (s, 2H), 6.36 (s, 1H), 7.25 (m, 5H), 7.71 (m, 2H), 7.77 (m, 2H). *m/z*: 446 $(M + 1)^+$.

2-(Aminomethyl)-3-(benzyloxy)-1-[2-(dimethylamino)ethyl]-6-methylpyridin-4(1*H*)-one (18). A solution of 5 mL of methanol containing 500 mg (1.12 mmol) of **17** and 69.91 μL (71.94 mg, 2.24 mmol) of hydrazine hydrate was refluxed overnight. The solution was allowed to cool to room temperature, inducing precipitation of side products. Cooling to 0 °C in an ice/water bath and adjusting the solution to pH 1 using concentrated hydrochloric acid led to a complete precipitation of the side products, which were removed from the solution by filtration. The filtrate was evaporated to dryness and dissolved in 5 mL of water. By use of a 10 M sodium hydroxide solution, the aqueous mixture was adjusted to pH 8, avoiding product precipitation, and added directly to the dimethyl sulfoxide solution of the activated fluorescein derivative **7** for fluorophor coupling.

4(and 5)-[(3-Benzyloxy-1-[2-(dimethylamino)ethyl]-6-methyl-4-oxopyridin-2-yl)methylcarbamoyl]-2-(3-hydroxy-6-oxo-6*H*-xanthen-9-yl)benzoic Acid (19). An analogous reaction as described for **8** using a basic aqueous solution of **18** gave **19** (367 mg, 0.54 mmol, 41%). *m/z*: 674 $(M + 1)^+$.

4(and 5)-[(1-[2-(Dimethylamino)ethyl]-3-hydroxy-6-methyl-4-oxopyridin-2-yl)methylcarbamoyl]-2-(3-hydroxy-6-oxo-6*H*-xanthen-9-yl)benzoic acid (20). An analogous procedure starting with 50 mg (0.74 mmol) of **19** as described for **9** gave **20**. Purity of the compound was verified by two different HPLC methods (for data, see Supporting Information). Method A had the following parameters: reversed phase C_{18} column, isocratic method, water/0.1% TFA (buffer A) and acetonitrile (buffer B). Method B had the following parameters: reversed phase C_{18} column, gradient, aqueous 1-heptanesulfonic acid (5 mM), pH 2 (HCl) (buffer A), and acetonitrile (buffer B) (21 mg, 0.03 mmol, 46%). *m/z*: 584 $(M + 1)^+$.

Acknowledgment. This work was supported by a fellowship for S.F. within the postdoctoral program of the German Academic Exchange Service (DAAD). M.P. is a MRC PhD Studentship holder, and U.E.S. is supported by the Wolfson Research Fellowship by the Royal Society. The authors thank Prof. Albert Haas for kindly providing tracers for colocalization studies.

Supporting Information Available: HPLC results of **9** and **20** and metal selectivity data of **9**. This material is available free of charge via the Internet at http://pubs.acs.org.

References

(1) Lippard, S. J.; Berg, J. M. *Principles of Bioinorganic Chemistry*; University Science Books: Mill Valley, CA, 1994.
(2) Kaim, W.; Schwederski, B. *Bioinorganic Chemistry*, 2nd ed.; B. G. Teubner: Stuttgart, Germany, 1995.
(3) Halliwell, B.; Gutteridge, J. M. C. Role of free radicals and catalytic metal ions in human disease: an overview. *Methods Enzymol.* **1990**, *186*, 1–85.
(4) Halliwell, B.; Gutteridge, J. M. C. Biologically relevant metal ion-dependent hydroxyl radical generation. An update. *FEBS Lett.* **1992**, *307*, 108–112.
(5) Gaeta, A.; Hider, R. C. The crucial role of metal ions in neurodegeneration: the basis for a promising therapeutic strategy. *Br. J. Pharmacol.* **2005**, *146*, 1041–1059.
(6) Molina-Holgado, M.; Hider, R. C.; Gaeta, A.; Williams, R.; Francis, P. Metals ions and neurodegeneration. *BioMetals*, in press.
(7) Bacon, B. R.; Britton, R. S. Hepatic injury in chronic iron overload. Role of lipid peroxidation. *Chem.-Biol. Interact.* **1989**, *70*, 183–226.
(8) Bacon, B. R.; Britton, R. S. The pathology of hepatic iron overload: a free radical-mediated process. *Hepatology* **1990**, *11*, 127–137.
(9) Kehrer, J. P. The Haber−Weiss reaction and mechanisms of toxicity. *Toxicology* **2000**, *149*, 43–50.
(10) Kowdley, K. V. Iron, hemochromatosis, and hepatocellular carcinoma. *Gastroenterology* **2004**, *127*, S79–S86.
(11) Valko, M.; Rhodes, C. J.; Moncol, J.; Izakovic, M.; Mazur, M. Free radicals, metals and antioxidants in oxidative stress-induced cancer. *Chem.-Biol. Interact.* **2006**, *1*, 1–40.
(12) Valko, M.; Leibfritz, D.; Moncol, J.; Cronin, M. T. D.; Mazur, M.; et al. Free radicals and antioxidants in normal physiological functions and human disease. *Int. J. Biochem. Cell Biol.* **2007**, *39*, 44–84.

(13) Petrat, F.; De Groot, H.; Rauen, U. Subcellular distribution of chelatable iron: a laser scanning microscopic study in isolated hepatocytes and liver endothelial cells. *Biochem. J.* **2001**, *356*, 61–69.
(14) Yu, Z.; Persson, H. L.; Eaton, J. W.; Brunk, U. T. Intralysosomal iron: a major determinant of oxidant-induced cell death. *Free Radical Biol. Med.* **2003**, *34*, 1243–1252.
(15) Kurz, T.; Leake, A.; von Zglinicki, T.; Brunk, U. T. Lysosomal redox-active iron is important for oxidative stress-induced DNA damage. *Ann. N.Y. Acad. Sci.* **2004**, *1019*, 285–288.
(16) Kurz, T.; Leake, A.; von Zglinicki, T.; Brunk, U. T. Relocalized redox-active lysosomal iron is an important mediator of oxidative-stress-induced DNA damage. *Biochem. J.* **2004**, *378*, 1039–1045.
(17) Terman, A.; Gustafsson, B.; Brunk, U. T. The lysosomal-mitochondrial axis theory of postmitotic aging and cell death. *Chem.-Biol. Interact.* **2006**, *163*, 29–37.
(18) Kurz, T.; Gustafsson, B.; Brunk, U. T. Intralysosomal iron chelation protects against oxidative stress-induced cellular damage. *FEBS J.* **2006**, *273*, 3106–3117.
(19) Persson, H. L.; Yu, Z.; Tirosh, O.; Eaton, J. W.; Brunk, U. T. Prevention of oxidant-induced cell death by lysosomotropic iron chelators. *Free Radical Biol. Med.* **2003**, *34*, 1295–1305.
(20) Horackova, M.; Ponka, P.; Byczko, Z. The antioxidant effects of a novel iron chelator salicylaldehyde isonicotinoyl hydrazone in the prevention of H_2O_2 injury in adult cardiomyocytes. *Cardiovasc. Res.* **2000**, *47*, 529–536.
(21) Simunek, T.; Boer, C.; Bouwman, R. A.; Vlasblom, R.; Versteilen, A. M. G.; et al. SIH, a novel lipophilic iron chelator, protects H9c2 cardiomyoblasts from oxidative stress-induced mitochondrial injury and cell death. *J. Mol. Cell. Cardiol.* **2005**, *39*, 345–354.
(22) Petrat, F.; Rauen, U.; De Groot, H. Determination of the chelatable iron pool of isolated rat hepatocytes by digital fluorescence microscopy using the fluorescent probe phen green SK. *Hepatology* **1999**, *29*, 1171–1179.
(23) Petrat, F.; De Groot, H.; Rauen, U. Determination of the chelatable iron pool of single intact cells by laser scanning microscopy. *Arch. Biochem. Biophys.* **2000**, *376*, 74–81.
(24) Glickstein, H.; El, R. B.; Link, G.; Breuer, W.; Konijn, A. M.; et al. Action of chelators in iron-loaded cardiac cells: accessibility to intracellular labile iron and functional consequences. *Blood* **2006**, *108*, 3195–3203.
(25) Glickstein, H.; El, R. B.; Shvartsman, M.; Cabantchik, Z. I. Intracellular labile iron pools as direct targets of iron chelators: a fluorescence study of chelator action in living cells. *Blood* **2005**, *106*, 3242–3250.
(26) Petrat, F.; Weisheit, D.; Lensen, M.; De Groot, H.; Sustmann, R.; et al. Selective determination of mitochondrial chelatable iron in viable cells with a new fluorescent sensor. *Biochem. J.* **2002**, *362*, 137–147.
(27) Rauen, U; Springer, A; Weisheit, D; Petrat, F; H.G, K. Assessment of chelatable mitochondrial iron by using mitochondrion-selective fluorescent iron indicators with different iron-binding affinities. *ChemBioChem* **2007**, *8*, 341–352.
(28) Ma, Y.; Luo, W.; Quinn, P. J.; Liu, Z. D.; Hider, R. C. Design, synthesis, physicochemical properties, and evaluation of novel iron chelators with fluorescent sensors. *J. Med. Chem.* **2004**, *47*, 6349–6362.
(29) Luo, W.; Ma, Y.; Quinn, P. J.; Hider, R. C.; Liu, Z. Design, synthesis and properties of novel iron(III)-specific fluorescent probes. *J. Pharm. Pharmacol.* **2004**, *56*, 529–536.
(30) Ma, Y.; De Groot, H.; Liu, Z.; Hider, R. C.; Petrat, F. Chelation and determination of labile iron in primary hepatocytes by pyridinone fluorescent probes. *Biochem. J.* **2006**, *395*, 49–55.
(31) Kaufmann, A. M.; Krise, J. P. Lysosomal sequestration of amine-containing drugs: analysis and therapeutic implications. *J. Pharm. Sci.* **2007**, *96*, 729.
(32) Mitsunobu, O. The use of diethyl azodicarboxylate and triphenylphosphine in synthesis and transformation of natural products. *Synthesis* **1981**, *1*, 28.
(33) Zhou, T.; Neubert, H.; Liu, D. Y.; Liu, Z. D.; Ma, Y.; et al. Iron binding dendrimers: a novel approach for the treatment of haemochromatosis. *J. Med. Chem.* **2006**, *49*, 4171–4182.
(34) Rae, T. D. Undetectable intracellular free copper: the requirement of a copper chaperone for superoxide dismutase. *Science* **1999**, *284*, 805–808.
(35) Liu, Z. D.; Khodr, H. H.; Liu, D. Y.; Lu, S. L.; Hider, R. C. Synthesis, physicochemical characterization, and biological evaluation of 2-(1′-hydroxyalkyl)-3-hydroxypyridin-4-ones: novel iron chelators with enhanced pFe^{3+} values. *J. Med. Chem.* **1999**, *42*, 4814–4823.
(36) Wis Vitolo, L. M.; Hefter, G. T.; Clare, B. W.; Webb, J. Iron chelators of the pyridoxal isonicotinoyl hydrazone class part II. Formation constants with iron(III) and iron(II). *Inorg. Chim. Acta* **1990**, *170*, 171–176.
(37) Zanker, V.; Peter, W. Die prototropen formen des fluoresceins. *Chem. Ber.* **1958**, *91*, 572–580.
(38) Sjöback, R.; Nygren, J.; Kubista, M. Absorption and fluorescence of fluorescein. *Spectrochim. Acta A* **1995**, *51*, L7–L21.
(39) Alvarez-Pez, J. M.; Ballesteros, L.; Talavera, E.; Yguerabide, J. Fluorescein excited-state proton exchange reactions: nanosecond emission kinetics and correlation with steady-state flurescence intensity. *J. Phys. Chem. A* **2001**, *105*, 6320–6332.
(40) Klonis, N.; Sawyer, W. H. Spectral properties of the prototropic forms of fluorescein in aqueous solution. *J. Fluoresc.* **1996**, *6*, 147–157.
(41) Liu, Z. D.; Liu, D. Y.; Hider, R. C. Iron Chelator Chemistry. *Iron Chelation Therapy*; Kluwer Academic/Plenum Publishers: New York, 2002; pp 141−166.
(42) Fakih, S.; Podinovskaia, M.; Kong, X. L.; Schaible, U. E.; Collins, H. L.; Monitoring intracellular labile iron pools: a novel fluorescent iron(III) sensor as a potentially advanced and non-invasive diagnosis tool. *J. Pharm. Sci.*, in press.
(43) Tenopoulou, M.; Kurz, T.; Doulias, P. T.; Galaris, D.; Brunk, U. T. Does the calcein-AM method assay the total cellular "labile iron pool" or only a fraction of it? *Biochem. J.* **2007**, *403*, 261.
(44) Gans, P.; Sabatini, A.; Vacca, A. Determination of equilibrium constants from spectrophotometric data obtained from solutions of known pH: the program pHab. *Ann. Chim.* **1999**, *89*, 45–49.
(45) Gans, P.; O'Sullivan, B. GLEE, a new computer program for glass electrode calibration. *Talanta* **2000**, *51*, 33–37.

JM8001247